nature microbiology

ARTICLES

https://doi.org/10.1038/s41564-018-0333-1

Gut pathobionts underlie intestinal barrier dysfunction and liver T helper 17 cell immune response in primary sclerosing cholangitis

Nobuhiro Nakamoto[1], Nobuo Sasaki[1,2], Ryo Aoki[1,3], Kentaro Miyamoto[1,4], Wataru Suda[5,6], Toshiaki Teratani[1], Takahiro Suzuki[1,4], Yuzo Koda[1,7], Po-Sung Chu[1], Nobuhito Taniki[1], Akihiro Yamaguchi[1], Mitsuhiro Kanamori[5], Nobuhiko Kamada[8], Masahira Hattori[6,9], Hiroshi Ashida[10], Michiie Sakamoto[11], Koji Atarashi[5,12], Seiko Narushima[5,12], Akihiko Yoshimura[5], Kenya Honda[5,12], Toshiro Sato[1*] and Takanori Kanai[1,2*]

Primary sclerosing cholangitis (PSC) is a chronic inflammatory liver disease and its frequent complication with ulcerative colitis highlights the pathogenic role of epithelial barrier dysfunction. Intestinal barrier dysfunction has been implicated in the pathogenesis of PSC, yet its underlying mechanism remains unknown. Here, we identify *Klebsiella pneumonia* in the microbiota of patients with PSC and demonstrate that *K. pneumoniae* disrupts the epithelial barrier to initiate bacterial translocation and liver inflammatory responses. Gnotobiotic mice inoculated with PSC-derived microbiota exhibited T helper 17 (T_H17) cell responses in the liver and increased susceptibility to hepatobiliary injuries. Bacterial culture of mesenteric lymph nodes in these mice isolated *K. pneumoniae*, *Proteus mirabilis* and *Enterococcus gallinarum*, which were prevalently detected in patients with PSC. A bacterial-organoid co-culture system visualized the epithelial-damaging effect of PSC-derived *K. pneumoniae* that was associated with bacterial translocation and susceptibility to T_H17-mediated hepatobiliary injuries. We also show that antibiotic treatment ameliorated the T_H17 immune response induced by PSC-derived microbiota. These results highlight the role of pathobionts in intestinal barrier dysfunction and liver inflammation, providing insights into therapeutic strategies for PSC.

Primary sclerosing cholangitis (PSC) is a chronic cholestatic liver disease characterized by the development of bile-duct strictures and the destruction of biliary trees that lead to end-stage liver cirrhosis[1–4]. Although the pathophysiology of PSC remains unknown, a frequent observation of portal bacteraemia[5] and elevated levels of endotoxin in cholangiocytes[6] suggested the implication of gut microbiota in PSC. Although gut microbiota is normally confined in the intestinal lumen, once the epithelial barrier is disrupted, the influx of gut microbiota can elicit T helper 17 (T_H17) immune response, resembling the liver inflammation in PSC[7]. As >70% of PSC is complicated with ulcerative colitis (UC)[1,2], colonic inflammation is a plausible cause of the barrier dysfunction; however, the majority of patients with UC are devoid of PSC[8,9], suggesting an additional layer of complexity. Recently, it is becoming apparent that PSC-associated UC (PSC/UC) shapes a distinct disease phenotype: PSC/UC typically exhibits discontinuous right-sided colitis, whereas classical UC is characterized by the continuous lesions originating from the rectum[10,11]. Interestingly, the gut microbiota of PSC/UC differed from those of classical UC and was rather similar to those of PSC without UC lesions[12–14]. Thus, it has been suggested that the dysbiosis contributed to the distinct disease phenotype of PSC/UC; however, it remains unexplored whether the emergence of specific bacterial species could induce bacterial translocation and subsequent progression to hepatobiliary inflammation. In this study, we generated gnotobiotic mice using faecal samples from patients with PSC/UC and identified the specific bacteria that are responsible for pathological bacterial translocation and subsequent T_H17 priming in the liver. Furthermore, using in vivo models and a two-dimensional organoid culture system, we have revealed a pathogenic mechanism by which multiple bacterial species collaboratively disrupt the intestinal epithelial barrier and induce T_H17 priming in the liver.

Results

T_H17 priming is induced in the livers of gnotobiotic mice inoculated with faecal samples from patients with PSC/UC. To determine the biological effects of gut microbiota on liver inflammation, we generated gnotobiotic mice by inoculating faecal samples derived

[1]Division of Gastroenterology and Hepatology, Department of Internal Medicine, Keio University School of Medicine, Shinanomachi, Tokyo, Japan. [2]AMED-CREST, Japan Agency for Medical Research and Development, Tokyo, Japan. [3]Institute of Health Science, Ezaki Glico Co., Ltd, Osaka, Japan. [4]Miyarisan Pharmaceutical Co., Ltd, Tokyo, Japan. [5]Department of Microbiology and Immunology, Keio University School of Medicine, Shinanomachi, Tokyo, Japan. [6]Laboratory of Metagenomics, Department of Computational Biology and Medical Sciences, The University of Tokyo, Chiba, Japan. [7]Research Unit/Immunology & Inflammation, Sohyaku Innovative Research Division, Mitsubishi Tanabe Pharma Corporation, Kanagawa, Japan. [8]Division of Gastroenterology, Department of Internal Medicine, University of Michigan, Ann Arbor, MI, USA. [9]Cooperative Major in Advanced Health Science, Graduate School of Advanced Science and Engineering, Faculty of Science and Engineering, Waseda University, Tokyo, Japan. [10]Department of Bacterial Infection and Host Response, Graduate School of Medical and Dental Sciences, Tokyo Medical and Dental University, Tokyo, Japan. [11]Department of Pathology, Keio University School of Medicine, Shinanomachi, Tokyo, Japan. [12]RIKEN Center for Integrative Medical Sciences, Laboratory for Gut Homeostasis, Kanagawa, Japan. *e-mail: t.sato@a7.keio.jp; takagast@z2.keio.jp

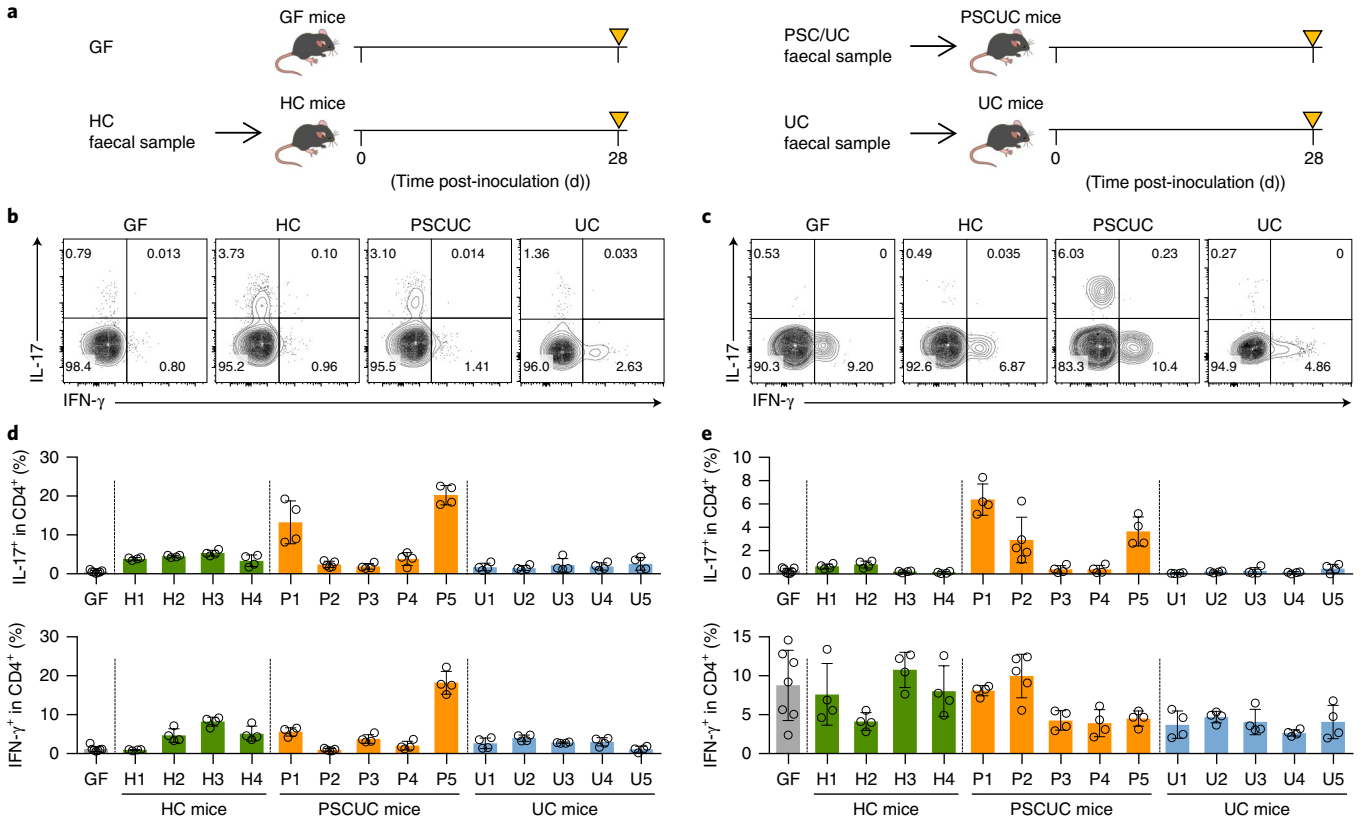

Fig. 1 | Magnitude of T_H17 priming in the liver and colon of gnotobiotic mice transplanted with human faecal samples. a, Study design: faecal samples derived from healthy controls (HC mice), patients with PSC/UC (PSCUC mice) or patients with UC (UC mice) were inoculated into GF mice, followed by immunological phenotyping at day 28 post-inoculation. The yellow triangles represent the time point of analysis. **b**,**c**, Representative intracellular IFN-γ and IL-17 staining of $CD3^+CD4^+$-gated cells in the colon (**b**) and liver (**c**) of mice from the indicated groups (GF: $n=7$; HC: $n=16$; PSCUC: $n=21$; and UC: $n=20$ mice). **d**,**e**, Frequency of IL-17$^+$ (T_H17) cells (upper) and IFN-γ$^+$ (T_H1) cells (lower) in $CD3^+CD4^+$-gated cells in the colon (**d**) and liver (**e**) of mice inoculated with faecal samples from HC1–4, PSC/UC1–5 and UC1–5 individuals, compared with GF mice (GF: $n=7$; H1–H4, P1, P3–P5 and U1–U5: $n=4$; and P2: $n=5$ mice). Data show the mean ± s.e.m. Data are combined from several independent experiments.

from patients with PSC/UC (PSCUC mice), patients with UC (UC mice) or healthy controls (HCs; HC mice) (Fig. 1a). Although the overall microbiota composition in human donors was not completely recapitulated in gnotobiotic mice, correlation analysis of principal coordinates from unweighted UniFrac distance indicated that dominant microbial taxonomy was conserved between human donors and corresponding gnotobiotic mice (Supplementary Fig. 1a,b). After stable colonization of the human gut microbiota, we examined T cell profiles in the livers and colons of the gnotobiotic mice (Fig. 1b,c). As previously described[15], T_H17 priming was induced in the colon, but not in the liver, of HC mice (Fig. 1d,e). Interestingly, three out of five PSC/UC patient-derived mouse groups exhibited potent T_H17 priming in the liver (Fig. 1e). We also observed significant upregulation of inflammatory genes, including serum amyloid A and interleukin-1β (IL-1β) in both the colons and livers of PSCUC mice (Supplementary Fig. 1c,d), suggesting that the PSC/UC patient-derived microbiota induced liver inflammation.

PSCUC mice are more susceptible to 3,5-dicarbethoxy-1,4-dihydrocollidine-induced hepatobiliary damage. Despite prominent T_H17 priming, faecal transplantation was insufficient to induce histological or serological changes in the liver of PSCUC mice even after a long colonization period of 90 days (Supplementary Fig. 2a–d). Thus, we questioned whether dysbiosis could promote 3,5-diethoxycarbonyl-1,4-dihydrocollidine (DDC)-fed hepatobiliary injury that has been used as a PSC disease model[16–18] (Fig. 2a). Although DDC induced rather mild hepatobiliary injury under germ-free conditions, gnotobiosis of HC microbiota enhanced the disease activity, suggesting an implication of gut microbiota in the progression of liver inflammatory lesions (Fig. 2b). Interestingly, DDC-fed PSCUC mice showed a higher level of serum total bilirubin and alkaline phosphatase, and T_H17 response in the liver than DDC-fed germ-free (GF) or HC mice (Fig. 2b–d). Pathological assessment revealed periductal fibrosis in PSCUC mice, a characteristic feature of PSC (Fig. 2e,f). We also confirmed significant upregulation of fibrosis marker gene expression in DDC-fed PSCUC mice (Fig. 2g). These observations provided the first prospective evidence that gut microbiota from PSC/UC promotes the hepatobiliary injury along with the liver T_H17 response.

Gnotobiotic mice with PSC/UC microbiota identified specific bacterial species associated with PSC/UC. Gnotobiotic PSCUC mice showed increased levels of serum endotoxin, indicating bacterial translocation (Fig. 3a). To identify the specific pathobionts responsible for bacterial translocation, we harvested the livers, mesenteric lymph nodes (MLNs) and spleens from gnotobiotic mice (Fig. 3b). Strikingly, we successfully isolated bacterial clones from the MLNs, whereas no bacteria could be grown from the liver or spleen of PSCUC gnotobiotic mice, or from any organs of specific pathogen-free (SPF), HC or UC gnotobiotic mice (Fig. 3b). Sequencing of 16S rRNA identified these bacteria as *Klebsiella pneumoniae*, *Proteus mirabilis* and *Enterococcus gallinarum*. To validate

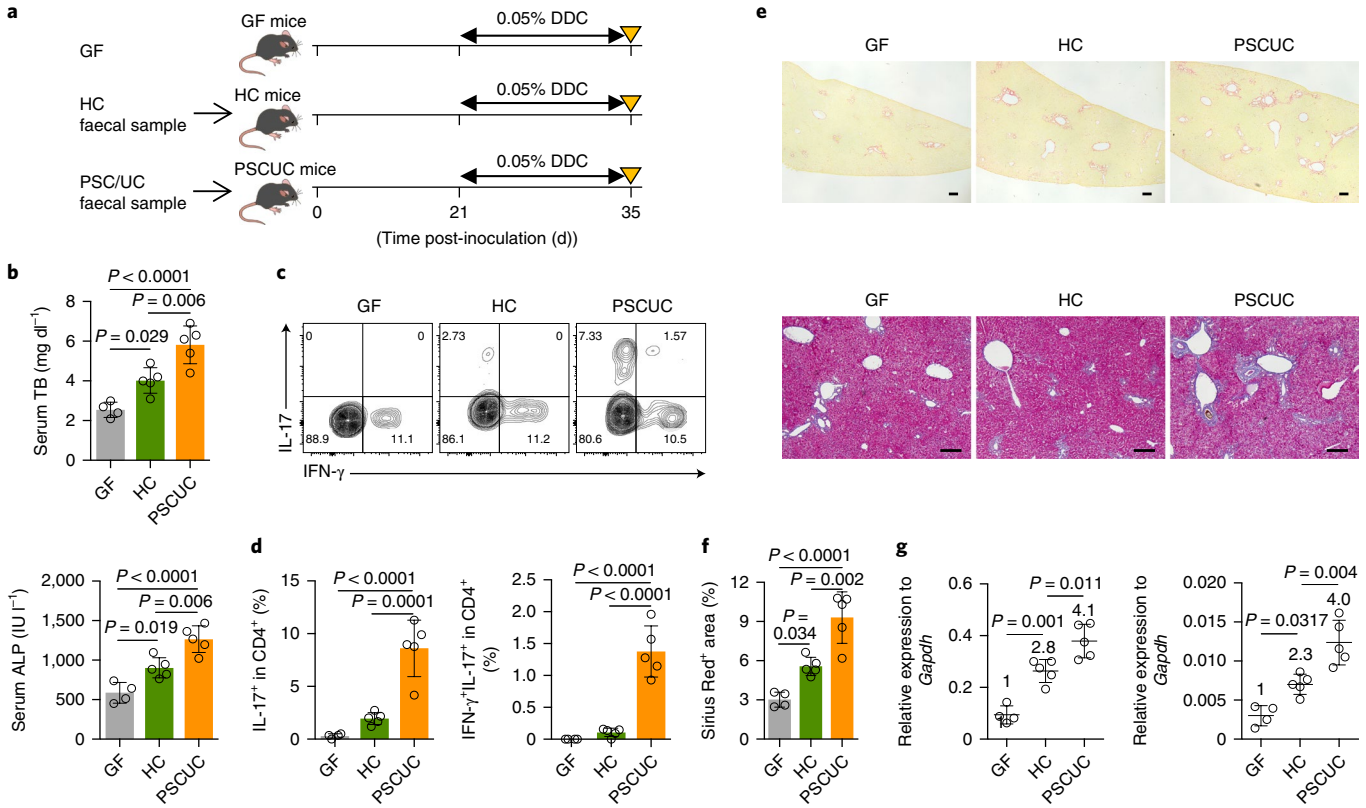

Fig. 2 | Increased susceptibility to DDC-induced hepatobiliary injury in PSCUC mice. a, Study design: GF mice, GF mice inoculated with HC faecal samples (HC mice) or PSC/UC faecal samples (PSCUC mice) were administered 0.05% DDC for 2 weeks from day 21 to day 35. The yellow triangles represent the time point of analysis. **b**, Serum total bilirubin (TB) (top) and alkaline phosphatase (ALP) (bottom) levels of mice from the indicated groups. **c**,**d**, Representative intracellular IFN-γ and IL-17 staining of $CD3^+CD4^+$-gated cells (**c**), and the frequency of $IL\text{-}17^+$ cells (left) and $IFN\text{-}\gamma^+IL\text{-}17^+$ cells (right) in $CD3^+CD4^+$ T cells (**d**) in the livers of mice from the indicated groups. **e**, Representative photomicrographs of Sirius Red (upper) and Masson trichrome (lower) staining of the liver sections of mice. Scale bars, 100 μm. **f**, Quantitative Sirius Red-positive area of the liver sections of mice from the indicated groups. **g**, qRT–PCR analysis of *Col1a1* (left) and *Timp1* (right) relative to *Gapdh* in the whole liver of mice from the indicated groups. The numbers in each graph indicate the ratio compared to GF mice. For **b**–**g**, $n = 4$ mice in the GF group and $n = 5$ mice in the other groups. For **b**, **d**, **f** and **g**, data show the mean ± s.e.m. ANOVA using Tukey's multiple-comparison correction was applied. Data are representative of two independent experiments.

the capability of bacterial translocation among these three bacteria, we reinoculated a mixture of the three bacteria (hereafter, 3-mix bacteria) into GF mice. Consistent with the result of PSCUC mice, gnotobiotic mice with the 3-mix bacteria (3-mix gnotobiotic mice) exhibited efficient bacterial translocation into the MLN but not into the liver as determined by bacterial culturing, PCR and fluorescence in situ hybridization (FISH) (Supplementary Fig. 3a,b). The failure of bacterial translocation detection in the liver was not due to a low sensitivity, because translocated bacteria were detected in the liver from mice that had been administered 3-mix bacteria by intravenous injection. These results suggested that 3-mix bacteria are sufficient to induce bacterial translocation in gnotobiotic mice.

We next determined whether these bacteria are prevalent in PSC/UC using collection of faecal samples comprising 18 patients with PSC/UC, 16 patients with classic UC and 10 HCs (Supplementary Table 1). The metagenome analyses depicted a drastic change of microbiota between HC and UC, reflecting colonic inflammation, but the difference between PSC/UC and classic UC was less evident (Supplementary Fig. 4a–c). Nevertheless, linear discriminant analysis effect size analysis identified the genera *Klebsiella* and *Enterococcus* as uniquely enriched bacterial species that corresponded to the 3-mix bacteria (Supplementary Fig. 4d). Furthermore, species-specific quantitative PCR (qPCR) analyses for *K. pneumoniae*, *P. mirabilis* and *E. gallinarum* revealed a clear difference of their prevalence among the groups. Notably, 17 out of 18 patients with PSC harboured *K. pneumoniae*, which was a significantly higher rate than that of HCs (0 out of 10) and patients with classic UC (5 out of 16), with $P < 0.0001$ and $P < 0.0002$ by Fisher's exact test, respectively (Fig. 3c). Likewise, the detection of *E. gallinarum* was higher in patients PSC than in those in the other groups. The high prevalence of these bacterial species was validated in other independent cohorts of faecal samples from 27 Japanese patients with PSC[19] and from 44 European patients with PSC[20] (Supplementary Fig. 5). We additionally examined faecal specimens collected from patients with other autoimmune liver diseases, including autoimmune hepatitis (AIH) and primary biliary cholangitis (PBC). Of note, *K. pneumoniae* was detected in 3 out of 9 and 5 out of 10 of faecal specimens from patients with AIH and PBC, respectively (Fig. 3d), suggesting that the prevalence of *K. pneumoniae* might be related to the presence of hepatobiliary diseases. Nevertheless, our results indicated that the 3-mix bacteria isolated from patients with PSC promoted bacterial translocation in the gnotobiotic mouse model, underscoring the pathogenic role of gut microbiota in PSC.

The 3-mix bacteria cooperatively promote the hepatobiliary disease progression through the T_H17 response. We next determined whether PSC-derived 3-mix bacterial strains are responsible for liver inflammation. Consistent with the result of PSCUC mice, 3-mix gnotobiotic mice showed a strong T_H17 response in the colon

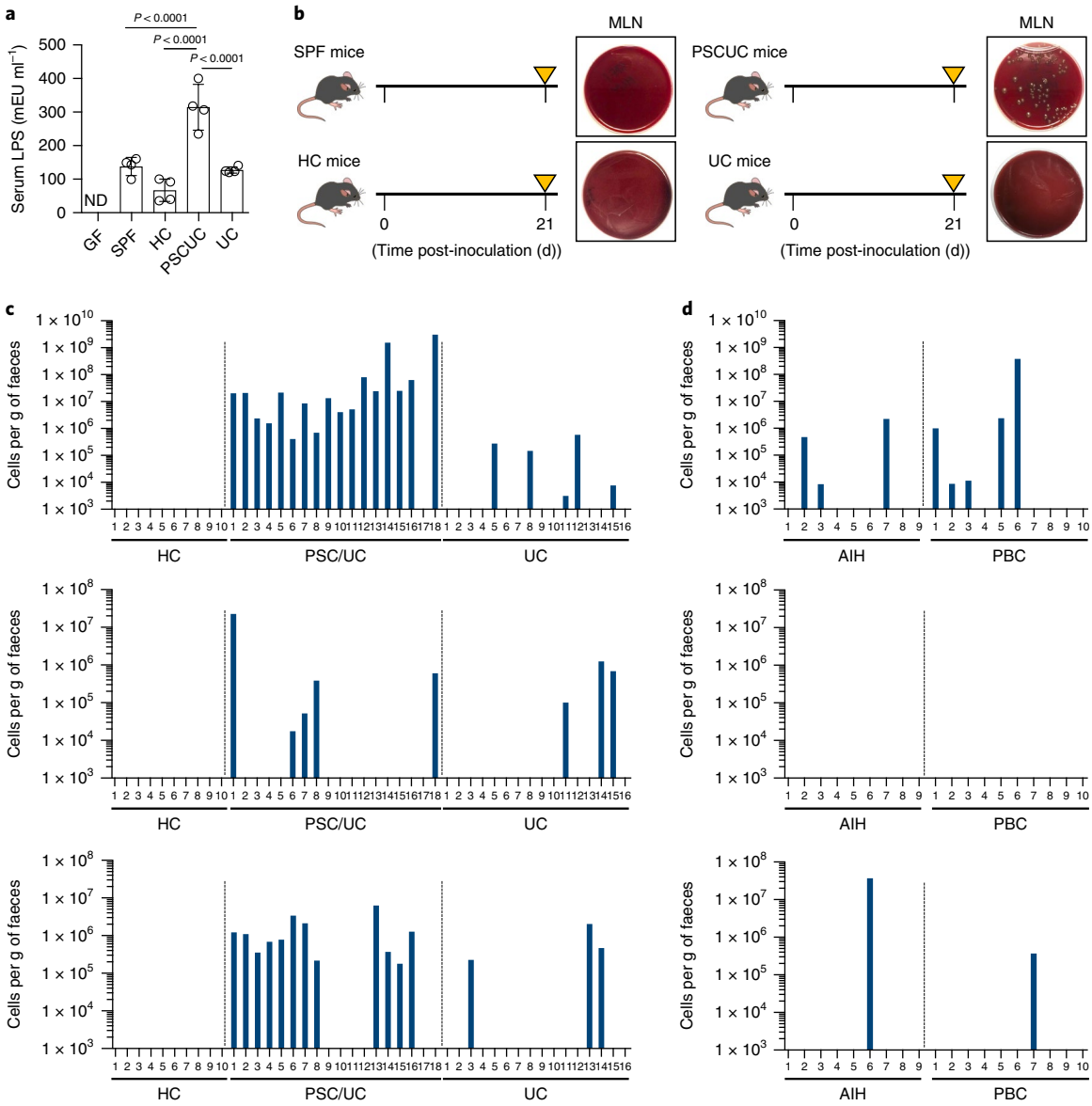

Fig. 3 | Gnotobiotic mice with PSC/UC microbiota identified specific bacterial species associated with PSC/UC from the MLN. a, Serum LPS concentration. $n = 3$ mice in the GF group and $n = 4$ mice in the SPF, HC, PSCUC and UC groups. ND, not detected. Data show the mean ± s.e.m. ANOVA using Tukey's multiple-comparison correction was applied. **b**, Study design: the liver, MLN and spleen were aseptically collected from the mice of each group on day 21 post-inoculation, followed by in vitro culture. The yellow triangles represent the time point of analysis. Representative photographs of the agar plates on the second day after colonization with the collected MLN are also shown. **c**, Amount of *K. pneumoniae* (upper), *P. mirabilis* (middle) and *E. gallinarum* (lower) in faecal samples from HC1–10, PSC/UC1–18 and UC1–16 individuals assessed by 16S qPCR. **d**, Amount of *K. pneumoniae* (upper), *P. mirabilis* (middle) and *E. gallinarum* (lower) in faecal samples from AIH1–9 and PBC1–10 individuals assessed by 16S qPCR.

and liver (Fig. 4a). To further determine which bacterial species is responsible for T_H17 priming, we inoculated GF mice with three bacterial strains either individually or in combination. Interestingly, the mono-colonization of *K. pneumoniae* or dual-colonization of *P. mirabilis* and *E. gallinarum* was less efficient in T_H17 induction than the 3-mix bacteria, suggesting that 3-mix bacteria cooperatively induced the liver inflammatory response (Fig. 4a). Accordingly, when stimulating naive $CD4^+$ T cells with heat-killed 3-mix bacteria, we observed higher T_H17 induction than when *K. pneumoniae* was used alone (Fig. 4b). These results suggest that, whether viable, the 3-mix bacteria could elicit T_H17 responses in the liver.

To address whether the liver T_H17 response contributes to the disease progression, we developed a therapeutic approach that targets T_H17 differentiation in the DDC-fed 3-mix gnotobiotic mouse model. As a single use of anti-IL-17A antibody failed in the amelioration of the hepatobiliary injury (Fig. 4c), we utilized RAR-related orphan receptor-γt (ROR-γt) inverse agonist (RIA) that has been previously shown to selectively inhibit T_H17 differentiation[21] (Fig. 4d). As expected, RIA treatment significantly reduced the number of T_H17 cells without affecting the numbers of T_H1 cells, confirming the specific inhibition of T_H17 differentiation (Fig. 4e,f). Importantly, RIA treatment also improved hepatobiliary injury and fibrosis of DDC-fed 3-mix gnotobiotic mice, emphasizing the pathogenic role of T_H17 activation in liver inflammation (Fig. 4g–j).

***K. pneumoniae* derived from the MLNs of PSCUC mice induces pore formation in human intestinal epithelial cells in vitro**. To obtain direct evidence of whether the 3-mix bacteria

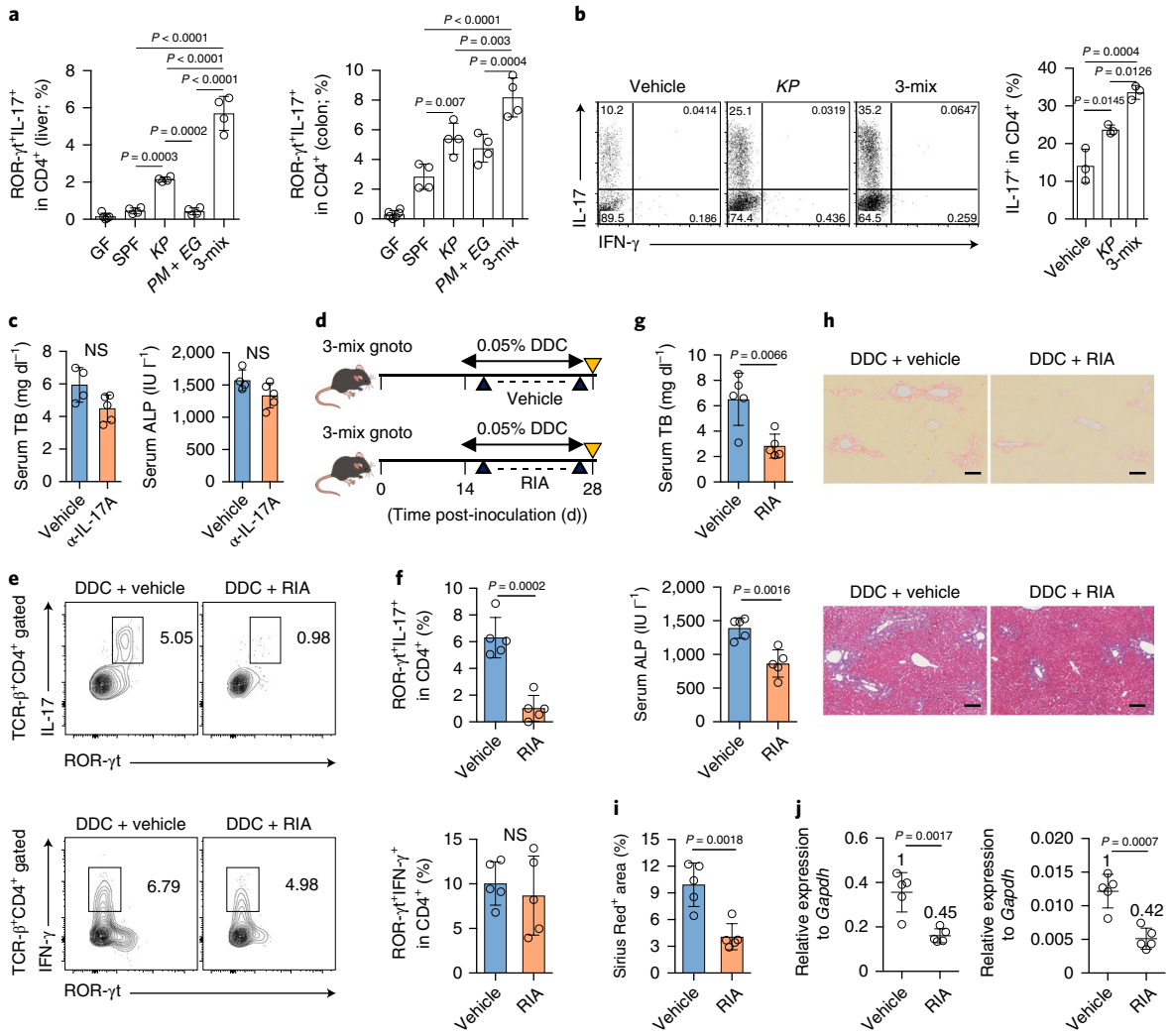

Fig. 4 | Inhibition of ROR-γt protects mice from DDC-induced hepatobiliary injury. a, Frequency of ROR-γt$^+$IL-17$^+$ cells in the liver (left) and colon (right) of mice inoculated with three bacterial strains either individually or in combination ($n=6$ mice in the GF group and $n=4$ mice in the other groups). Data show the mean ± s.e.m. Data are representative of two independent experiments. *PM*, *P. mirabilis*; *EG*, *E. gallinarum*. **b**, Naive CD4 T cells and dendritic cells were cultured with *K. pneumoniae* (*KP*) alone or with the 3-mix culture under the T_H17-skewing condition. Left: representative dot plots of intracellular IFN-γ and IL-17 staining on CD11c$^-$CD4$^+$-gated cells restimulated with PMA and ionomycin. Right: the frequency of IL-17A$^+$IFN-γ$^-$ cells in CD11c$^-$CD4$^+$ cells in each condition. Data show the mean ± s.e.m. ($n=3$ biological replicates). For **a** and **b**, ANOVA using Tukey's multiple-comparison correction was applied. **c**, 3-mix gnotobiotic mice were intraperitoneally given either an anti-mouse IL-17A-neutralizing antibody (500 μg per mice, $n=4$ mice) or mouse IgG1 isotype control ($n=5$ mice) every other day for 2 weeks during DDC feeding from day 14 to day 28 post-transplantation. Serum TB (left) and ALP (right) levels are shown. **d**, Study design: 3-mix gnotobiotic (gnoto) mice fed with DDC were treated daily with either a RIA (10 mg per kg mice) or vehicle for 2 weeks. The yellow triangles represent the time point of analysis. **e**,**f**, Representative intracellular ROR-γt and IL-17 staining (upper) and ROR-γt and IFN-γ staining (lower) of TCR-β$^+$CD4$^+$-gated cells (**e**), and the frequency of IL-17$^+$ cells (upper) and IFN-γ$^+$ cells (lower) in TCR-β$^+$CD4$^+$ T cells (**f**) in the liver of mice. **g**, Serum TB (upper) and ALP (lower) levels of mice. **h**, Representative photomicrographs of Sirius Red staining (upper) and Masson trichrome staining (lower) of the liver sections of mice. Scale bars, 100 μm. **i**, Quantitative Sirius Red-positive area of the liver sections of mice. **j**, qRT–PCR analysis of *Col1a1* (left) and *Timp1* (right) relative to *Gapdh* in the whole liver of mice. The numbers in each graph indicate the ratio compared to the vehicle group. For **e**–**j**, $n=5$ mice per group. For **c**, **f**, **g**, **i** and **j**, data show the mean ± s.e.m. Two-sided Student's *t*-test was applied. NS, not significant.

penetrated the intestinal epithelial barrier, we next performed FISH analysis using intestinal mucosa of 3-mix gnotobiotic mice. Although no bacterium invaded the intestinal mucosa of SPF mice, bacterial DNA was detected underneath the intestinal epithelium in 3-mix gnotobiotic mice, indicating the presence of bacterial invasion. The mucosal bacterial DNA was also detected in single *K. pneumoniae* gnotobiotic mice, but not in *P. mirabilis* + *E. gallinarum* gnotobiotic mice, highlighting the essential role of *K. pneumoniae* in the bacterial invasion (Fig. 5a and Supplementary Fig. 6a).

To clarify the mechanism of how microbiota interacts with the intestinal epithelial barrier, we established a monolayered culture system using human intestinal organoids. Contrary to the closed apical sides in conventional organoids, the monolayered organoids directly exposed their apical sides to culture medium, allowing interactions between the administered bacteria and the epithelial surface[22,23] (Fig. 5b). We obtained two different *K. pneumoniae* strains, *KP*-P1 and *KP*-P5, which were derived from the MLN of PSCUC mice generated from two independent patients. Interestingly, upon administering *KP*-P1 and *KP*-P5 on the monolayered organoids,

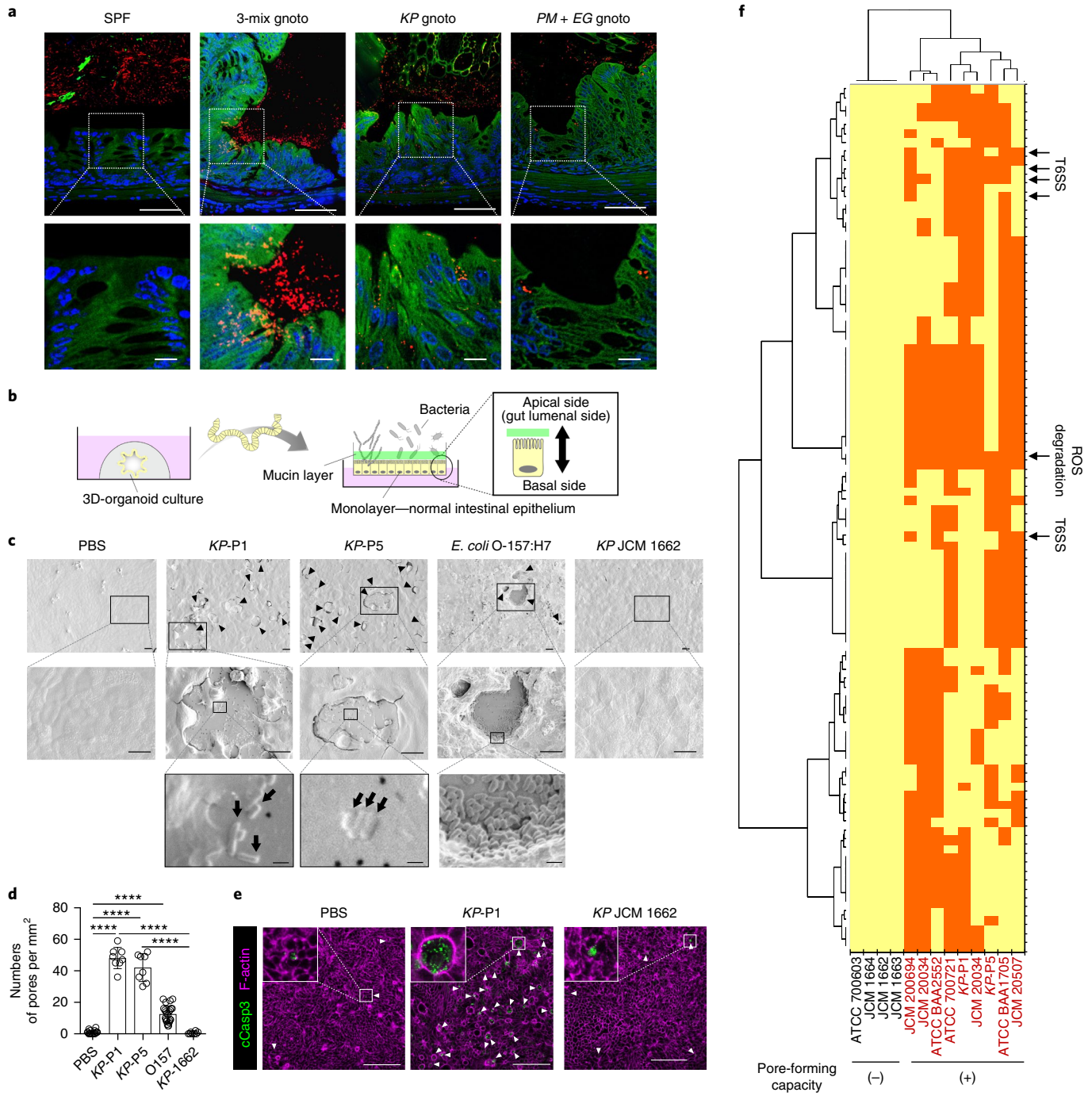

Fig. 5 | *K. pneumoniae* derived from the MLNs of PSCUC mice induces epithelial pore formation of colonic epithelial cells. **a**, Representative FISH staining of the ileum of mice from the indicated groups ($n = 4$ mice per group) to identify the bacterial 16S rRNA genes (red), co-stained with phalloidin (F-actin; green) and 4′,6-diamidino-2-phenylindole (DAPI; blue). Insets show higher magnification. Scale bars, 50 μm in the upper panels and 10 μm in the lower panels. **b**, Schematic drawing of the two-dimensional organoid microbiome interaction system used in this experiment. **c**,**d**, Representative scanning electron microscopy images (**c**) and the quantitative scoring of damaged intestinal epithelium with pores (>10 μm; epithelial pore) (**d**) of the intestinal epithelium after 8 h of culture of *KP*-P1 or *KP*-P5, enterohemorrhagic *E. coli* O157, a non-pore-forming *K. pneumoniae* strain JCM 1662^T provided from RIKEN (*KP*-1662) and the PBS control. The middle and lower panels in **c** show each upper image at a higher magnification. Arrowheads indicate collapsed colonic monolayers. Microorganisms are indicated by the arrows. Scale bars, 20 μm in the top and middle panels and 2 μm in the lower panels. For **c** and **d**, $n = 16$ independent samples in the PBS group, $n = 8$ samples in the *KP*-P1, *KP*-P5 and *KP*-1662 groups and $n = 24$ samples in the O157 group. For **d**, data show the mean ± s.e.m. $^{****}P < 0.0001$ by ANOVA using Tukey's multiple-comparison correction. **e**, Intestinal epithelial cells co-cultured with the indicated bacterial strain were stained with the anti-active caspase-3 antibody (green) and co-stained with phalloidin (F-actin; pink). Arrowheads represent epithelial pores, and the inset shows a higher magnification of an epithelial pore. Scale bars, 100 μm. Data are representative of four independent experiments. **f**, Comparative analysis of the whole genomes of the tested 13 *K. pneumoniae* strains revealed that 97 orthologous genes correlated with the pore-forming capacity, defined as present (orange) in more than 4 of 9 pore-forming *K. pneumoniae* strains (+) and defective (yellow) in all 4 non-pore-forming *K. pneumoniae* strains (–). Detailed information about the gene ID for each row is listed in Supplementary Table 4. ROS, reactive oxygen species; T6SS, type VI secretion system.

both bacteria induced the formation of epithelial pores in the monolayer within 8 h (Fig. 5c,d). A similar phenotype was observed using a strain of enterohemorrhagic *Escherichia coli* O157:H7 (Fig. 5c,d). Immunostaining illustrated that epithelial pores were filled with cleaved caspase-3$^+$ apoptotic cells and encircled by viable epithelial cells (Fig. 5e). Furthermore, RNA sequencing (RNA-seq) analysis revealed marked upregulation of genes related to apoptotic and inflammatory pathways in *KP*-P1-stimulated epithelial cells compared to JCM 1662-stimulated epithelial cells (Supplementary Fig. 6b,c and Supplementary Table 2). Heat-killed *K. pneumoniae* failed to induce epithelial pore formation (Supplementary Fig. 6d). These results suggested that *K. pneumoniae* may induce epithelial pore formation through apoptotic and inflammatory signalling in a contact-dependent manner. Interestingly, the epithelial pore-inducing capacity of *K. pneumoniae* varied among the strains, of which seven strains induced pore formation, whereas four did not (Fig. 5c and Supplementary Fig. 6e).

To gain genetic insights into epithelial pore-forming capacity of *K. pneumoniae*, we obtained metagenome data from 13 strains of *K. pneumoniae*. There was no correlation between epithelial pore-forming capacity and multilocus sequencing typing based on virulence genes or capsular (K) typing (Supplementary Table 3). Interestingly, the whole-genome phylogenetic analysis revealed that *K. pneumoniae* strains with epithelial pore-forming capacity were widely distributed, whereas those without epithelial pore-forming capacity tended to be closely related (Supplementary Fig. 7). Furthermore, 97 orthologous genes associated with epithelial pore-forming capacity were identified by comparative analysis of the whole-genome sequencing of 13 *K. pneumoniae* strains, including genes involved in the type VI secretion system[24,25] and reactive oxygen species degradation (Fig. 5f and Supplementary Table 4). These results suggested that the epithelial pore-forming capacity of *K. pneumoniae* is determined by strain-specific genotype.

Epithelial pore-forming capacity in a *K. pneumoniae* strain was responsible for bacterial translocation and subsequent T_H17 priming in the liver. To determine whether the in vitro epithelial pore-forming capacity correlates to in vivo barrier disruption, we performed fluorescein isothiocyanate (FITC)-conjugated dextran (FITC-dextran) leakage analysis. In gnotobiote with epithelial pore-inducing *K. pneumoniae*, 4 kDa FITC-dextran, but not 70 kDa FITC-dextran, leaked to the systemic circulation, indicating the presence of barrier disruption that allows the penetration of small particles into the mucosa (Fig. 6a). Of note, the increased leakage was not detected in gnotobiote with non-epithelial pore-inducing *K. pneumoniae* (JCM 1662^T), indicating that the epithelial pore-forming capacity contributes to in vivo barrier disruption. The association between *K. pneumoniae* and intestinal barrier function prompted us to investigate whether the epithelial-damaging effect of *K. pneumoniae* contributed to liver inflammation. Thus, we generated gnotobiotic mice with modified 3-mix strains (m3-mix gnotobiotic mice) in which *K. pneumoniae* was replaced with the non-pore-forming strain (Fig. 6b). In contrast to 3-mix gnotobiotic mice, m3-mix gnotobiotic mice were devoid of mucosal barrier invasion (Fig. 6c) and showed lower serum endotoxin levels (Fig. 6d). Furthermore, m3-mix gnotobiotic mice exhibited considerably lower levels of liver T_H17 priming (Fig. 6e,f). These results suggested that the epithelial-damaging effect of *K. pneumoniae* is crucial for the induction of the liver T_H17 response.

We next determined whether the presence of pore-forming capacity affects liver inflammation in the DDC model. Interestingly, m3-mix gnotobiotic mice showed significantly decreased liver dysfunction compared to that in 3-mix gnotobiotic mice, highlighting the pathogenic effect of pore-forming capacity (Fig. 6g). Because the microbiota may affect the cholestatic phenotype by modulating the DDC metabolism, we decided to employ taurocholic acid (TCA)-induced hepatobiliary injury, as another disease model for PSC (Fig. 6h). Interestingly, TCA feeding caused intrahepatic cholestasis-mediated liver enzyme level elevation in SPF mice, but the hepatobiliary dysfunction was minimal in GF mice, suggesting the involvement of gut microbiota in this model. Consistent with the DDC model, 3-mix gnotobiotic mice, but not m3-mix gnotobiotic mice, developed severe hepatobiliary injury along with increased T_H17 response (Fig. 6i–m). Pathological assessment revealed periductal inflammation and fibrotic change in interlobular bile ducts in 3-mix gnotobiotic mice. Importantly, we noted that the infiltration of inflammatory cells and fibrotic response were involved with larger bile ducts, which is a characteristic of PSC (Fig. 6l). These results further reinforced the biological effect of pore-forming *K. pneumoniae* on hepatobiliary injuries.

Treatment with metronidazole or vancomycin ameliorated T_H17 responses in the liver. To determine whether antibiotic treatment could modulate liver immune responses in our experimental model, we generated gnotobiotic mice using faecal samples from a patient with PSC (P5) that harboured *K. pneumoniae* and *E. gallinarum*, and treated the mice with metronidazole or vancomycin that possess antibacterial potential against *K. pneumoniae* and *E. gallinarum*, respectively[26,27] (Supplementary Fig. 8a,b). Notably, the T_H17 response was induced in P5-PSCUC gnotobiotic mice and the immune response was significantly decreased by metronidazole or vancomycin treatment (Supplementary Fig. 8c,d). The fact that vancomycin treatment decreased the T_H17 response suggests that, in addition to *K. pneumoniae*, there may be vancomycin-sensitive microbiota that possess epithelium-disrupting capability. Nevertheless, these results not only underscored the involvement of *K. pneumoniae* and *E. gallinarum* in hepatobiliary inflammation but also provide preclinical evidence for a feasible pathobionts-targeting therapeutic strategy for PSC.

Discussion

Recent microbiome studies revealed an association between dysbiosis and PSC; however, the mechanistic understanding of how gut microbiota contribute to the pathogenesis of PSC remained elusive. In this study, by combining gnotobiote and classical bacterial culturing, we successfully isolated *K. pneumoniae*, *P. mirabilis* and *E. gallinarum* from the MLN of gnotobiotic mice. These 3-mix bacteria were found to be prevalent in patients with PSC and responsible for bacterial translocation and subsequent hepatobiliary inflammation in the gnotobiotic mouse models.

It has been reported that bacterial translocation is frequently associated with hepatobiliary diseases[28,29], and intestinal barrier dysfunction has been considered as its pathological basis[30]. In this study, we first demonstrated that PSC-derived *K. pneumoniae* possess epithelial-damaging abilities that contribute to bacterial translocation. Interestingly, members of the Enterobacteriaceae family, including *K. pneumoniae*, were often observed in the microbiota of individuals with hepatobiliary diseases, such as liver cirrhosis[28,31] and PBC[32]. Furthermore, the abundance of the bacteria in PBC was associated with bacterial invasion of epithelial cells[32]. These results collectively highlighted the previously unappreciated link between bacterial translocation and the Enterobacteriaceae family in hepatobiliary diseases. Our monolayered-organoid culture system further revealed that PSC/UC-derived *K. pneumoniae* can induce epithelial pore formation in the epithelial layer. In accordance with this, the epithelial pore-forming capacity was associated with intestinal barrier dysfunction in vivo, providing insights into the interplay between gut microbiota and bacterial translocation in PSC. Interestingly, the pore-forming capacity of *K. pneumoniae* was strain specific and enabled a comparative whole-genome analysis. The genetic analysis did not identify conserved virulent toxins, but listed several candidate genes responsible for pore-forming

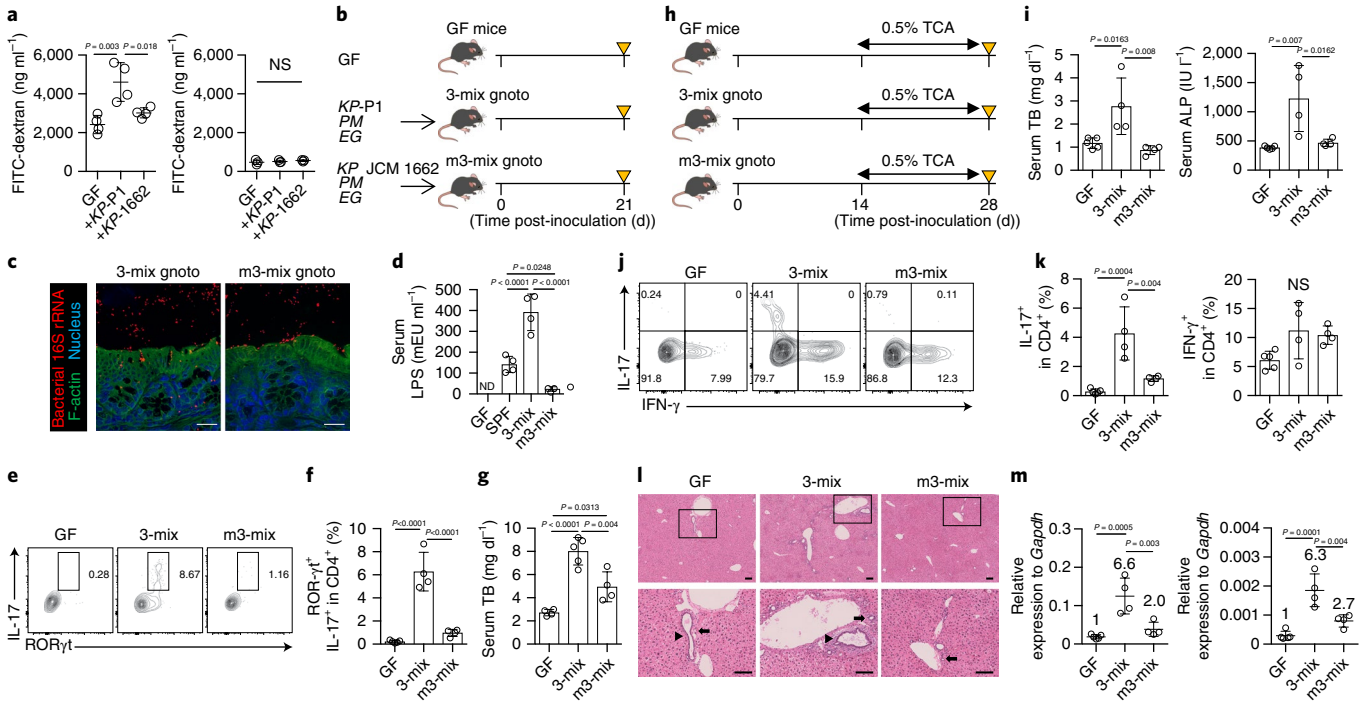

Fig. 6 | Bacterial translocation and T_H17 priming in the liver are dependent on *K. pneumoniae* strains. a, Serum FITC-dextran (4 kDa (left) and 70 kDa (right)) concentration calculated 8 h following mono-colonization with *KP*-P1 or *KP*-1662 to GF mice ($n = 4$ mice per group for 4 kDa and $n = 3$ mice per group for 70 kDa). **b**, Study design: 3-mix strains derived from the MLNs of PSCUC1 mice or m3-mix were inoculated into GF mice, followed by immunological phenotyping at day 21. The yellow triangles represent the time point of analysis. **c**, Representative FISH staining of the ileum of mice ($n = 3$ mice per group) to identify the bacterial 16S rRNA genes, co-stained with phalloidin (F-actin) and DAPI (nucleus). Scale bars, 20 μm. **d**, Serum LPS concentration of mice. **e**,**f**, Representative intracellular ROR-γt and IL-17 staining on $CD3^+CD4^+$-gated cells (**e**), and the frequency of ROR-$γt^+$IL-17^+ cells (**f**) in the liver of mice. For **d**–**f**, $n = 5$ mice in the GF group and $n = 4$ mice in the other groups. **g**, Mice inoculated with the indicated bacteria were administered 0.05% DDC for 2 weeks from day 14 to day 28. Serum TB levels are shown ($n = 4$ mice in the GF and m3-mix groups, and $n = 5$ mice in 3-mix group). **h**, Study design: mice in the indicated groups were administered 0.5% TCA for 2 weeks from day 14 to day 28. **i**, Serum TB (left) and ALP (right) levels. **j**,**k**, Representative intracellular IFN-γ and IL-17 staining of TCR-$β^+CD4^+$-gated cells (**j**), and the frequency of IL-17^+ cells (left) and IFN-$γ^+$ cells (right) in TCR-$β^+CD4^+$ T cells (**k**) in the liver of mice. **l**, Representative photomicrographs of haematoxylin and eosin staining of the liver sections of mice. Insets show higher magnification. The arrows and arrowheads indicate interlobular bile ducts and larger bile ducts, respectively. Scale bars, 100 μm. **m**, qRT-PCR analysis of *Col1a1* (left) and *Timp1* (right) relative to *Gapdh* in the whole liver. The numbers in each graph indicate the ratio compared to GF mice. For **i**–**m**, $n = 5$ mice in the GF group and $n = 4$ mice in the other groups. For **a**, **d**, **f**, **g**, **i**, **k** and **m**, data show the mean ± s.e.m. ANOVA using Tukey's multiple-comparison correction was applied.

capacity, including the type VI secretion system. The type VI secretion system is a contact-dependent protein secretion system known to transfer various effector proteins to target host cells[33,34], and thus may contribute to the *K. pneumoniae*-induced epithelial pore formation demonstrated in this study. Further studies will be required to identify and confirm the genetic factors responsible for the epithelial pore-forming capacity in *K. pneumoniae*.

Although we successfully isolated bacteria from the MLN of PSCUC mice, no bacteria could be grown from the liver. This was in contrast to the frequent observation of translocated bacteria in the liver of patients with PSC[7]. There is a possibility that the translocated bacteria were immediately eliminated by immune cells upon reaching the liver; however, this scenario seems unlikely because we failed to detect any bacterial signal using FISH and PCR. A more plausible explanation is that a 'gut–vascular barrier'[35] blocked the invaded bacteria from translocating into the liver. Indeed, 4 kDa but not 70 kDa FITC-dextran was able to reach the systemic circulation, supporting the intact gut–vascular barrier hypothesis in the 3-mix gnotobiotic mice. It is tempting to speculate that disruption of this second firewall by comorbid colitis allows escalation of bacterial translocation and in turn activates the liver T_H17 response in PSC. Interestingly, the gnotobiotic mice with PSC/UC-derived microbiota or 3-mix bacteria establish hepatic T_H17 responses even in the absence of bacterial translocation to the liver. Instead, we observed increased endotoxin levels in the serum of the mice, suggesting that a disrupted epithelial barrier promoted an influx of microbial components and/or by-products to the liver. As heat-killed 3-mix bacteria were able to promote T_H17 differentiation, the delivery of the 3-mix bacteria-derived products to the liver may be sufficient to induce hepatic T_H17 responses. Taken together, our findings suggest that the gut microbiota is responsible for the disruption of the first intestinal epithelial barrier, and a second trigger, such as colitis or hepatobiliary injury, further consolidates the T_H17-mediated disease progression in PSC.

The infiltration of T_H17 cells in the PSC liver was previously reported[7], yet the activation mechanism of T_H17 differentiation has not been determined. In this study, using a gnotobiotic system, we demonstrated that PSC/UC microbiota was able to induce T_H17 differentiation in the liver. The comparable level of T_H17 induction was achieved by a colonization of 3-mix bacteria but not by the mono-colonization of *K. pneumoniae*, suggesting that pathobionts cooperatively induced liver inflammation. Interestingly, we demonstrated that elimination of these pathobionts was effective in reducing the number of T_H17 cells in the liver. Consistent with our

results, a recent report demonstrated that antibiotics-based eradication of *E. gallinarum* alleviated the progression of extra-intestinal autoimmune diseases[36]. Furthermore, one pilot clinical trial demonstrated the therapeutic effect of metronidazole and vancomycin on PSC[37]. These results collectively suggested that the gut microbiota is implicated in hepatobiliary inflammation, and larger clinical trials will be warranted to establish the antibiotics-based therapeutic approach to PSC.

We also found that the gut microbiota-inducible T_H17 response was crucial for hepatobiliary disease progression and was therapeutically targetable in PSC disease models. We noted that antibody-based inhibition of IL-17A was insufficient to block the disease progression of the DDC-fed PSCUC model, reminiscent of a failure in a clinical trial for IBD[38,39]. This failure may be attributed to the residual production of other cytokines from T_H17 cells, such as IL-17F and granulocyte–macrophage colony-stimulating factor[40]. To circumvent this complexity, we employed therapeutic targeting of ROR-γt, an essential master transcription factor for T_H17 differentiation[41–43]. Interestingly, the RIA efficiently blocked the pathobiont-induced hepatic T_H17 response and ameliorated the DDC-induced hepatobiliary injury in PSCUC mice. These results provided evidence that pharmacological inhibition of T_H17 differentiation could be a therapeutic approach for PSC.

In summary, the current study identified disease-modulating pathobionts from patients with PSC/UC. One of the key functions of these pathobionts is to disrupt the intestinal epithelial barrier through the strain-specific epithelial-damaging effect of *K. pneumoniae*, which enables collateral translocation of other pathobionts and elicits subsequent T_H17 priming in the MLN and liver. Our results collectively provide insights into the implication of the gut microbiota in the disease pathogenesis of PSC.

Methods

Patients. HCs ($n=10$) and patients with complications of PSC/UC ($n=18$), UC ($n=16$), AIH ($n=9$) and PBC ($n=10$) were included in this study. The diagnosis of PSC was made according to clinical guidelines and typical findings on cholangiography (endoscopic retrograde cholangiography and/or magnetic resonance cholangiopancreatography) or liver biopsy. The diagnosis of UC was based on a combination of endoscopy, histopathology and radiological and serological investigations. The diagnoses of AIH and PBC were made according to clinical guidelines and typical histological findings. The ethics committee at Keio University School of Medicine (Tokyo, Japan) approved the protocol (no. 20140211). The study was conducted according to the principles of the Helsinki Declaration II, and written informed consent was obtained from all study participants. The study is registered at the University Hospital Medical Information Network (UMIN) clinical trial registration system (UMIN 000018068).

Animals. Male GF mice (C57BL/6 background strain, 6–8-weeks old) were purchased from Sankyo Lab Service Corporation and were kept in the GF Facility of Keio University School of Medicine. Male C57BL/6 mice (6–8-weeks old) were purchased from Japan CLEA (Tokyo, Japan) and maintained under SPF conditions in Central Laboratories for Experimental Animals (Kawasaki, Japan) and the Animal Care Facility of Keio University School of Medicine. All experiments were approved by regional animal study committees and were performed during March 2015 to September 2018 according to the institutional guidelines and Home Office regulations.

Gnotobiotic study design. Faecal samples from PSC/UC, UC and HC individuals were collected after having obtained written informed consent. Faecal samples were suspended in equal volumes (w/v) of PBS containing 40% glycerol, snap-frozen and stored at −80 °C until use. The frozen stocks were thawed, suspended in 6-fold volumes of PBS and passed through a 70-μm cell strainer. GF mice were orally inoculated with 200 μl of the suspensions using a stainless-steel feeding needle. Experiments were conducted after a colonization period of 3–4 weeks or after a longer period of 12 weeks. We initially tested faecal samples obtained from each disease group (4–5 per group) to confirm that the composition of microbiota used for the gnotobiotic studies is representative of each group by the unweighted UniFrac analysis. In some experiments, GF mice transplanted with human stool samples were given either metronidazole (1 g l^{-1}) or vancomycin (500 mg l^{-1}) in drinking water 1 day after the inoculation for 21 days. To confirm the existence of any bacteria outside the intestine of SPF mice or humanized gnotobiotic mice, the liver, MLN and spleen were carefully harvested and anaerobically cultured on blood liver, BHI and reinforced clostridial medium agar plates. The isolates were identified with 16S rRNA gene sequencing. To examine the effects of each of the bacterial species, 1×10^8 colony-forming units of a single species were suspended in 200 μl of medium or a combination of mixed bacteria was suspended and then orally or intravenously administered to GF mice.

DDC-induced or TCA-induced experimental hepatobiliary inflammation and liver fibrosis. To induce hepatobiliary inflammation and liver fibrosis, GF mice or humanized gnotobiotic mice were freely fed a 0.05% DDC-enriched (Sigma-Aldrich) or 0.5% TCA-enriched (Tokyo Chemical industry) diet for 14 days, followed by serological, histological and immunological assessment. To inhibit T_H17 responses, a RIA, GSK805 (10 mg per kg mice; no. HY-12776, Medchemexpress) dissolved in 10% DMSO/90% corn oil, was orally administered to DDC-fed mice daily for 14 days[21,44]. To neutralize IL-17A, an anti-mouse IL-17A-neutralizing antibody (500 μg per mice; clone 17F3, no. BE0173, BioXcell) or mouse IgG1 isotype control (500 μg per mice; no. BE0083, BioXcell) was intraperitoneally administered to DDC-fed mice every other day for 14 days.

Bacterial strains and culture. *K. pneumoniae* JCM 1662^T, JCM 1663, JCM1664, JCM 20034, JCM 20348, JCM 20507 and JCM 20694 were obtained from the Japan Collection of Microorganisms (RIKEN BioResource Center, Wako, Japan). *K. pneumoniae* ATCC 700603, ATCC BAA1705, ATCC BAA2552 and ATCC 700721 were kindly provided by K.H., Keio University. *E. coli* O157:H7 was grown overnight in LB broth. *K. pneumoniae*, *P. mirabilis* and *E. gallinarum* were anaerobically cultured in BHI broth (BD). To prepare heat-killed bacteria, the bacteria were collected by centrifugation and washed three times with PBS. After washing, the bacteria were heat-killed at 95 °C for 30 min.

Human intestinal organoid culture. Normal colonic organoids were established from human patients and maintained as described in our previous work[45]. Long-term healthy intestinal organoids were embedded into Matrigel (Corning) and cultured in medium composed of Advanced DMEM/F12 supplemented with penicillin–streptomycin, 10 mM HEPES, 2 mM GlutaMAX, 1×B27 (Life Technologies), 1 mM *N*-acetylcysteine (Wako Pure Chemical Industries), 10 nM GastrinI (Sigma), 50 ng ml^{-1} human recombinant epidermal growth factor, 0.5 μM A83-01, 3 μM SB202190, 50% afamin–Wnt3a (Afm-W) complex condition medium (v/v)[46], R-spondin 1-condition medium (10% v/v) and noggin-condition medium (10% v/v).

Preparation of two-dimensional organoid microbiome interaction system. For the monolayer organoid culture, three-dimensional cultured human colonic organoids were maintained in Afm-W, R-spondin 1, noggin, epidermal growth factor, A83-01, SB202190 with 10 μM Y-27632 for at least 1 day before dissociation and then seeded onto 0.4-μm pore ThinCert 24-well plates (Greiner) coated with 10% Cellmatrix type I-C (Nitta Gelatin). At 2–3 days after seeding, the medium of the monolayer colonic organoids was replaced with differentiation condition medium without Afm-W, SB202190 and Y-27632. Prior to infection with bacteria, the colonic epithelium was washed in advanced DMEM/F12 and antibiotic-free differentiation condition medium was added. For the two-dimensional organoid microbiome interaction system, intestinal epithelia were co-cultured with 1×10^5 colony-forming units of each bacterium for 8 h.

Sample collection and DNA extraction. Fresh faecal samples were collected using stool collection tubes and an anaerobiosis generator was added to the samples to favour the preservation of anaerobic bacteria at the outpatient clinic of Keio University Hospital. The samples were processed immediately and frozen at −80 °C for bacterial preservation. Bacterial DNA was isolated as described previously[47]. In brief, bacterial DNA was isolated by the enzymatic lysis method using lysozyme (Sigma-Aldrich) and achromopeptidase (Wako). DNA samples were then purified by treating with ribonuclease A (Wako), followed by precipitation with 20% polyethylene glycol solution (PEG6000 in 2.5 M sodium chloride). DNA was then pelleted by centrifugation, rinsed with 75% ethanol and dissolved in Tris-EDTA buffer.

Faecal microbiota quantification by qPCR. Quantification of *K. pneumoniae* was performed using the *K. pneumonia*-EASY genesig kit (Primerdesign), PrecisionPLUS qPCR Master Mix (Primerdesign) and the Thermal Cycler Dice Real Time System II (Takara), according to the manufacturer's instructions. Quantification of *E. gallinarum* and *P. mirabilis* was performed using SYBR Premix EX Taq II (Takara) and the Thermal Cycler Dice Real Time System II. The primer sets used in this study were as follows: *E. gallinarum* forward 5′-TTACTTGCTGATTTTGATTCG-3′ and reverse 5′-TGAATTCTTCTTTGA AATCAG-3′ (ref. [48]); *P. mirabilis* forward 5′-GTTATTCGTGATGGTATGGG-3′ and reverse 5′-ATAAAGGTGGTTACGCCAGA-3′ (ref. [49]).

16S rRNA metagenomic analysis. The hypervariable V3–V4 region of the 16S gene was amplified using Ex Taq Hot Start (Takara Bio) and subsequently purified using AMPure XP (Beckman Coulter). Mixed samples were prepared by pooling approximately equal amounts of each amplified DNA and sequenced using the Miseq Reagent Kit V3 (600 Cycle) and Miseq sequencer (Illumina), according

to the manufacturer's instructions. Sequences were analysed using the QIIME software package version 1.9.1 (refs. [50,51]). Paired-end sequences were joined using a fastq-join tool in the ea-utils software package (https://doi.org/10.2174/1875036201307010001). High-quality sequences per sample (15,000) were randomly chosen from the quality filter-passed sequences. After trimming off both primer sequences using cutadapt (https://doi.org/10.14806/ej.17.1.200) followed by chimeras detection by the USEARCH[52] de novo method, the sequences were assigned to operational taxonomic units using the UCLUST algorithm[53] with a sequence identity threshold of 96%. Taxonomic assignments of each operational taxonomic unit were made by similarity searching against the publicly available 16S (RDP version 10.27 and CORE update 2 September 2012) and the NCBI genome database using the GLSEARCH program. The data were rarefied to 10,000 sequences per sample, as determined by the rarefaction curves. Relative abundances of the community members were determined using the rarefied data. UniFrac analysis was performed as described previously[54]. To determine bacterial taxonomy that explained differences between conditions, the linear discriminant analysis effect size method was used[55].

Localization of bacteria by FISH. Colon and ileal tissues containing faecal material were fixed with Carnoy's solution for 3 h. Paraffin-embedded sections were de-waxed and hydrated. The hybridization step was performed at 50 °C overnight with an EUB338 probe (5′-GCTGCCTCCCGTAGGAGT-3′, with an Alexa 555 label) diluted to a final concentration of 10 μg ml^{-1} in hybridization buffer (20 mM Tris-HCl, pH 7.4, 0.9 M NaCl, 0.1% SDS and 20% formamide). After washing for 10 min in wash buffer (20 mM Tris-HCl, pH 7.4, and 0.9 M NaCl) and three times for 10 min in PBS, samples were stained with phalloidin-iFluor 488 (Abcam). After washing three times for 10 min in PBS, slides were mounted using Prolong anti-fade mounting media with DAPI (Life Technologies). Microscopic observations were performed using a BIO-REVO BZ-9000 fluorescence microscope (Keyence).

Isolation of lymphocytes and flow cytometry. Liver and spleen mononuclear cells were separated as described previously[56]. Intestinal lamina propria mononuclear cells and MLN mononuclear cells were prepared as described previously[57]. After blocking with anti-Fc receptor (CD16/32, BD Pharmingen) for 20 min, the cells were incubated with the specific fluorescence-labelled monoclonal antibody at 4 °C for 30 min. The following monoclonal antibodies were used: anti-mouse anti-T cell receptor-β (TCR-β; no. 109228, Biolegend, peridinin chlorphyll protein–Cy5.5 conjugate, clone H57-597), anti-CD3e (no. 552774, BD Bioscience, phycoerythrin (PE)–Cy7 conjugate, clone 145-2C11), anti-CD4 (no. 563106, BD Bioscience, BV510 conjugate, clone RM4-5), anti-CD11b (no. 101245, Biolegend, BV510 conjugate, clone M1/70), anti-CD11c (no.558079, BD Bioscience, PE–Cy7 conjugate, clone HL3), anti-F4/80 (no. 123131, Biolegend, BV421 conjugate, clone BM8) and fixable viability dye eFluor780 (no. 65-0864-14, eBioscience). Events acquired with FACS Canto II (Becton Dickinson) were analysed with FlowJo software (Tree Star). For intracellular cytokine staining, cells were stimulated for 4 h with lipopolysaccharide (LPS; from *E. coli* B5; Sigma) or PMA (50 ng ml^{-1}; Sigma-Aldrich) and ionomycin (500 ng ml^{-1}; Sigma-Aldrich) in the presence of brefeldin A (10 μg ml^{-1}; BD Bioscience) or Golgistop (10 μg ml^{-1}; BD Bioscience), followed by surface staining, permeabilization and intracellular staining with anti-mouse anti-interferon-γ (IFN-γ; no. 554412, BD Bioscience, PE conjugate, clone XMG1.2; no. 11-7311-82, eBioscience, FITC conjugate, clone XMG1.2), anti-tumour necrosis factor-α (no. 554419, BD Bioscience, PE conjugate, clone MP6-XT22), anti-IL-1β (no. 17-7114-80, eBioscience, allophycocyanin (APC) conjugate, clone NJTEN3), anti-IL-17A (no. 560221, eBioscience, Alexa Fluor 488 conjugate, clone TC11-18H10), anti-IL-22 (no. 17-7222-82, eBioscience, APC conjugate, clone IL22JOP) and anti-ROR-γt (no. 562894, BD Bioscience, BV421 conjugate, clone Q31-378).

Serological and histological analysis. Serum levels of alanine aminotransferase, alkaline phosphatase and total bilirubin were measured using a LDH-UV kinetic method (SRL). Livers were fixed in 10% formalin, embedded in paraffin. Sections were stained with haematoxylin and eosin, Masson trichrome or Sirius Red for collagen staining and quantitative analysis of the fibrotic area was performed using the Image J software. Colon and ileal tissues were fixed in 10% formalin or Carnoy's solution and embedded in paraffin.

qPCR analysis. Total RNA was extracted from liver homogenates using the RNeasy Mini Kit (Qiagen). Complementary DNA was synthesized from 1 μg total RNA by reverse transcription. To determine the gene expression, PCR was performed using AmpliTaq Gold Fast PCR MasterMix (Applied Biosystems) and the following predesigned primers: *Gapdh* (Mm03302249_g1), *Saa1* (Mm00656927_g1), *Saa2* (Mm04208126_mH), *Saa3* (Mm00441203_m1), *Fut2* (Mm01205565_m1), *Reg3b* (Mm00440616_g1), *Reg3g* (Mm00441127_m1), *Il1b* (Mm01336189_g1), *Col1a1* (Mm008016666_g1) and *Timp1* (Mm01341361_m1). To quantify the products, real-time PCR was performed using the TaqMan Universal Master Mix and StepOne Plus systems (Applied Biosystems). The level of target gene expression was normalized to *Gapdh* expression in each sample.

T_H17 differentiation from mice naive CD4 T cells. Bacterial culture supernatants were sterilized through a 0.22-μm pore size membrane filter. Naive CD4 T cells were prepared from the spleen and superficial lymph nodes using the CD4$^+$ T Cell Isolation Kit for mouse (Miltenyi Biotec). Naive CD4 T cells were then isolated using CD62L MicroBeads, mouse (Miltenyi Biotec). For preparation of dendritic cells, following lysis of red blood cells, splenocytes were blocked with anti-CD16/32 antibody (2.4G2) followed by incubation with CD11c MicroBeads, mouse (Miltenyi Biotec). Splenic dendritic cells were then isolated using the autoMACS system. Naive CD4 T cells (5×10^4 cells) and dendritic cells (2.5×10^3 cells) were cultured in a round-bottomed 96-well plate with bacterial culture supernatants (3% v/v of culture medium), in the presence of soluble anti-CD3e antibody under the T_H17-skewing condition (anti-IFN-γ: 5 mg ml^{-1}, anti-IL-4: 5 mg ml^{-1}, anti-IL-2: 2 mg ml^{-1}, IL-6: 20 ng ml^{-1} and transforming-growth factor-β: 0.5 ng ml^{-1}) in RPMI 1640 supplemented with 10% FBS, 1% penicillin–streptomycin mixed solution, 1× non-essential amino acids solution and 0.05 mM 2-ME. Four days later, cells were restimulated with PMA or ionomycin in the presence of brefeldin A for an additional 5 h. Following staining of cell surface CD4 and CD11c, cells were fixed and permeabilized and stained for intracellular IL-17A. Data were acquired by FACS Canto II and analysed with FlowJo software (Tree Star).

RNA-seq analysis. Total RNA was isolated from organoids using TRIzol reagent (Life Technologies). For RNA-seq, RNA library preparation was performed using a TruSeq RNA Sample Prep Kit v2 (Illumina) according to the manufacturer's instructions. Libraries were sequenced by Illumina HiSeq 4000 on the 100-bp paired-end mode. The sequenced reads were mapped to the human reference genome (NCBI 37.2) and normalized to fragments per kilobase per million reads (FPKM) values using the Tophat2 and Cufflinks software pipeline (https://doi.org/10.1186/gb-2013-14-4-r36 and https://doi.org/10.1038/nprot.2012.016). Gene Ontology and Kyoto Encyclopedia of Genes and Genomes (KEGG) pathway enrichment analysis was done with the DAVID tool (https://doi.org/10.1038/nprot.2008.211) on genes that were significantly differentially expressed.

Scanning electron microscopy analysis. Co-cultured intestinal epithelium with bacteria were fixed with 2.5% glutaraldehyde (TCI Chemicals) in PBS overnight at 4 °C. These samples were post-fixed for 1 h with 1% osmium tetroxide (TCI Chemicals) dissolved in PBS, dehydrated in a graded series of ethanol, coated with gold sputtering and observed under a VHX-D510 scanning electron microscope in the high vacuum mode (Keyence). In every experiment, the morphology of four independent positions in an intestinal epithelium was examined by scanning electron microscopy and the number of epithelial pores (>10 μm) were counted in each experiment. These experiments were repeated 3–6 times for statistical analysis.

Immunocytochemistry. Monolayered colonic epithelium was co-cultured with bacteria for 8 h in a 24-well transwell system. After incubation with bacteria or PBS control, cells were triple stained with cleaved caspase-3 antibody (1:400, Cell Signaling), the cell membrane dye (filamentous actin) phalloidin (1:300, Thermo Fisher) and the DNA dye Hoechst 33324 (1:1,000, Thermo Fisher), and apoptotic cells were observed using a confocal microscope (SP5, Leica).

Intestinal permeability in vivo. Mice were orally administered with 4 kDa FITC-dextran or 70 kDa FITC-dextran (Sigma-Aldrich) via a nasogastric tube after being fasted for 6 h. Blood samples were collected from the tail vein at 1 and 4 h post-administration. The concentration of FITC in the collected serum was measured using a spectrophotometer, according to the manufacturer's instructions. Serum from non-administered mice was used to determine the background.

Measurement of LPS concentration. ToxinSensor Chromogenic Limulus Amebocyte Lysate Endotoxin Assay Kit (GenScript) was used for determination of serum LPS concentrations, following the manufacturer's instructions. Briefly, samples were diluted 5-fold with endotoxin-free water. Limulus amebocyte lysate reagents were added to serum and incubated at 37 °C for 40 min. Subsequently, the absorbance at 540 nm was measured using the FilterMax F3 Multi-Mode Microplate Reader (Molecular Devices).

Bacterial genome sequencing. The genome sequences of *Klebsiella* strains were determined by the whole-genome shotgun strategy using PacBio RSII and Illumina MiSeq sequencers. The genomic DNA was sheared to obtain DNA fragments. Template DNA was prepared according to each supplier's protocol. Obtained RSII reads were subjected to de novo assembly using HGAP3. MiSeq reads (2 × 300 nt) were mapped onto the RSII-assembled contigs to correct low-quality regions. Phylogenetic trees were constructed based on the Mash distance[58] using the neighbour-joining method.

Multilocus sequencing typing, *wzi* and *wzc* sequence typing. The genomic sequences of each strain were aligned against the multilocus sequencing typing database (http://bigsdb.pasteur.fr/klebsiella/klebsiella.html). Sequence-based capsular (K) typing was carried out based on the sequencing of *wzi* or *wzc* genes[59,60].

Statistical analysis. Statistical analyses were performed using GraphPad Prism software version 6.0 (GraphPad software Inc.). Differences between two groups were evaluated using a two-sided Student's *t*-test or Wilcoxon rank-sum test. Comparison of more than two groups was performed by one-way analysis of variance (ANOVA), followed by Tukey's multiple-comparison test. Correlations were tested for significance by the Spearman rank correlation test. Proportions between the two groups were compared with Fisher's exact test. Differences at $P < 0.05$ were considered significant. Sample sizes were determined based on previous studies from our group and publication in this field. All animals were age and sex matched and randomly allocated to each group, and the investigators were not blinded during group allocation.

Reporting Summary. Further information on research design is available in the Nature Research Reporting Summary linked to this article.

Data availability

The data supporting the findings of this study are available from the corresponding authors upon request. 16S rRNA sequencing and whole-genome sequencing data have been deposited in the DNA Data Bank of Japan (DDBJ) database with the accession numbers DRA007475 and DRA007476 for 16S rRNA sequencing and PRJDB7545 for whole-genome sequencing. RNA sequencing data have been deposited in the European Genome-phenome Archive (EGA) database with the accession number EGAS00001003332.

Received: 11 September 2018; Accepted: 29 November 2018;
Published online: 14 January 2019

References

1. Lazaridis, K. N. & LaRusso, N. F. Primary sclerosing cholangitis. *N. Engl. J. Med.* **375**, 1161–1170 (2016).
2. Horsley-Silva, J. L., Carey, E. J. & Lindor, K. D. Advances in primary sclerosing cholangitis. *Lancet Gastroenterol. Hepatol.* **1**, 68–77 (2016).
3. Hirschfield, G. M., Karlsen, T. H., Lindor, K. D. & Adams, D. H. Primary sclerosing cholangitis. *Lancet* **382**, 1587–1599 (2013).
4. Dyson, J. K., Beuers, U., Jones, D. E. J., Lohse, A. W. & Hudson, M. Primary sclerosing cholangitis. *Lancet* **391**, 2547–2559 (2018).
5. O'Toole, A. et al. Primary sclerosing cholangitis and disease distribution in inflammatory bowel disease. *Clin. Gastroenterol. Hepatol.* **10**, 439–441 (2012).
6. Sasatomi, K., Noguchi, K., Sakisaka, S., Sata, M. & Tanikawa, K. Abnormal accumulation of endotoxin in biliary epithelial cells in primary biliary cirrhosis and primary sclerosing cholangitis. *J. Hepatol.* **29**, 409–416 (1998).
7. Katt, J. et al. Increased T helper type 17 response to pathogen stimulation in patients with primary sclerosing cholangitis. *Hepatology* **58**, 1084–1093 (2013).
8. Loftus, E. V. Jr, Sandborn, W. J., Lindor, K. D. & Larusso, N. F. Interactions between chronic liver disease and inflammatory bowel disease. *Inflamm. Bowel Dis.* **3**, 288–302 (1997).
9. Loftus, E. V. et al. PSC-IBD: a unique form of inflammatory bowel disease associated with primary sclerosing cholangitis. *Gut* **54**, 91–96 (2005).
10. Claessen, M. M. et al. More right-sided IBD-associated colorectal cancer in patients with primary sclerosing cholangitis. *Inflamm. Bowel Dis.* **15**, 1331–1336 (2009).
11. Karlsen, T. H. & Boberg, K. M. Update on primary sclerosing cholangitis. *J. Hepatol.* **59**, 571–582 (2013).
12. Sabino, J. et al. Primary sclerosing cholangitis is characterised by intestinal dysbiosis independent from IBD. *Gut* **65**, 1681–1689 (2016).
13. Kummen, M. et al. The gut microbial profile in patients with primary sclerosing cholangitis is distinct from patients with ulcerative colitis without biliary disease and healthy controls. *Gut* **66**, 611–619 (2017).
14. Iwasawa, K. et al. Characterisation of the faecal microbiota in Japanese patients with paediatric-onset primary sclerosing cholangitis. *Gut* **66**, 1344–1346 (2017).
15. Atarashi, K. et al. Th17 cell induction by adhesion of microbes to intestinal epithelial cells. *Cell* **163**, 367–380 (2015).
16. Pollheimer, M. J., Trauner, M. & Fickert, P. Will we ever model PSC?—"It's hard to be a PSC model!". *Clin. Res. Hepatol. Gastroenterol.* **35**, 792–804 (2011).
17. Tephly, T. R., Gibbs, A. H. & De Matteis, F. Studies on the mechanism of experimental porphyria produced by 3,5-diethoxycarbonyl-1,4-dihydrocollidine. Role of a porphyrin-like inhibitor of protohaem ferro-lyase. *Biochem. J.* **180**, 241–244 (1979).
18. Fickert, P. et al. A new xenobiotic-induced mouse model of sclerosing cholangitis and biliary fibrosis. *Am. J. Pathol.* **171**, 525–536 (2007).
19. Atarashi, K. et al. Ectopic colonization of oral bacteria in the intestine drives T_H1 cell induction and inflammation. *Science* **358**, 359–365 (2017).
20. Bajer, L. et al. Distinct gut microbiota profiles in patients with primary sclerosing cholangitis and ulcerative colitis. *World J. Gastroenterol.* **23**, 4548–4558 (2017).
21. Withers, D. R. et al. Transient inhibition of ROR-γt therapeutically limits intestinal inflammation by reducing T_H17 cells and preserving group 3 innate lymphoid cells. *Nat. Med.* **22**, 319–323 (2016).
22. In, J. et al. Enterohemorrhagic *Escherichia coli* reduce mucus and intermicrovillar bridges in human stemcell-derived colonoids. *Cell. Mol. Gastroenterol. Hepatol.* **2**, 48–62 (2016).
23. Sato, T. et al. Long-term expansion of epithelial organoids from human colon, adenoma, adenocarcinoma, and Barrett's epithelium. *Gastroenterology* **141**, 1762–1772 (2011).
24. Shneider, M. M. et al. PAAR-repeat proteins sharpen and diversify the type VI secretion system spike. *Nature* **500**, 350–353 (2013).
25. Russell, A. B., Peterson, S. B. & Mougous, J. D. Type VI secretion system effectors: poisons with a purpose. *Nat. Rev. Microbiol.* **12**, 137–148 (2014).
26. Siu, L. K., Yeh, K. M., Lin, J. C., Fung, C. P. & Chang, F. Y. *Klebsiella pneumoniae* liver abscess: a new invasive syndrome. *Lancet Infect. Dis.* **12**, 881–887 (2012).
27. Murray, B. E. The life and times of the *Enterococcus*. *Clin. Microbiol. Rev.* **3**, 46–65 (1990).
28. Wiest, R., Lawson, M. & Geuking, M. Pathological bacterial translocation in liver cirrhosis. *J. Hepatol.* **60**, 197–209 (2014).
29. Llorente, C. & Schnabl, B. The gut microbiota and liver disease. *Cell. Mol. Gastroenterol. Hepatol.* **1**, 275–284 (2015).
30. Miele, L. et al. Increased intestinal permeability and tight junction alterations in nonalcoholic fatty liver disease. *Hepatology* **49**, 1877–1887 (2009).
31. Steffen, E. K., Berg, R. D. & Deitch, E. A. Comparison of translocation rates of various indigenous bacteria from the gastrointestinal tract to the mesenteric lymph node. *J. Infect. Dis.* **157**, 1032–1038 (1988).
32. Tang, R. et al. Gut microbial profile is altered in primary biliary cholangitis and partially restored after UDCA therapy. *Gut* **67**, 534–541 (2018).
33. Jiang, F., Waterfield, N. R., Yang, J., Yang, G. & Jin, Q. A *Pseudomonas aeruginosa* type VI secretion phospholipase D effector targets both prokaryotic and eukaryotic cells. *Cell Host Microbe* **15**, 600–610 (2014).
34. Alcoforado Diniz, J., Liu, Y. C. & Coulthurst, S. J. Molecular weaponry: diverse effectors delivered by the type VI secretion system. *Cell. Microbiol.* **17**, 1742–1751 (2015).
35. Spadoni, I. et al. A gut–vascular barrier controls the systemic dissemination of bacteria. *Science* **350**, 830–834 (2015).
36. Manfredo Vieira, S. et al. Translocation of a gut pathobiont drives autoimmunity in mice and humans. *Science* **359**, 1156–1161 (2018).
37. Tabibian, J. H. et al. Randomised clinical trial: vancomycin or metronidazole in patients with primary sclerosing cholangitis—a pilot study. *Aliment. Pharmacol. Ther.* **37**, 604–612 (2013).
38. Hueber, W. et al. Secukinumab, a human anti-IL-17A monoclonal antibody, for moderate to severe Crohn's disease: unexpected results of a randomised, double-blind placebo-controlled trial. *Gut* **61**, 1693–1700 (2012).
39. Colombel, J. F., Sendid, B., Jouault, T. & Poulain, D. Secukinumab failure in Crohn's disease: the yeast connection? *Gut* **62**, 800–801 (2013).
40. McGeachy, M. J. GM-CSF: the secret weapon in the T_H17 arsenal. *Nat. Immunol.* **12**, 521–522 (2011).
41. Korn, T., Bettelli, E., Oukka, M. & Kuchroo, V. K. IL-17 and Th17 cells. *Annu. Rev. Immunol.* **27**, 485–517 (2009).
42. Ivanov, I. I. et al. The orphan nuclear receptor RORγt directs the differentiation program of proinflammatory IL-17$^+$ T helper cells. *Cell* **126**, 1121–1133 (2006).
43. Gaffen, S. L., Jain, R., Garg, A. V. & Cua, D. J. The IL-23–IL-17 immune axis: from mechanisms to therapeutic testing. *Nat. Rev. Immunol.* **14**, 585–600 (2014).
44. Xiao, S. et al. Small-molecule RORγt antagonists inhibit T helper 17 cell transcriptional network by divergent mechanisms. *Immunity* **40**, 477–489 (2014).
45. Fujii, M. et al. A colorectal tumor organoid library demonstrates progressive loss of niche factor requirements during tumorigenesis. *Cell Stem Cell* **18**, 827–838 (2016).
46. Mihara, E. et al. Active and water-soluble form of lipidated Wnt protein is maintained by a serum glycoprotein afamin/alpha-albumin. *eLife* **5**, e11621 (2016).
47. Nishijima, S. et al. The gut microbiome of healthy Japanese and its microbial and functional uniqueness. *DNA Res.* **23**, 125–133 (2016).
48. Jackson, C. R., Fedorka-Cray, P. J. & Barrett, J. B. Use of a genus- and species-specific multiplex PCR for identification of enterococci. *J. Clin. Microbiol.* **42**, 3558–3565 (2004).
49. Stankowska, D., Kwinkowski, M. & Kaca, W. Quantification of *Proteus mirabilis* virulence factors and modulation by acylated homoserine lactones. *J. Microbiol. Immunol. Infect.* **41**, 243–253 (2008).
50. Caporaso, J. G. et al. QIIME allows analysis of high-throughput community sequencing data. *Nat. Methods* **7**, 335–336 (2010).
51. Kuczynski, J. et al. Using QIIME to analyze 16S rRNA gene sequences from microbial communities. *Curr. Protoc. Bioinformatics* **36**, 10.7.1–10.7.20 (2011).

52. Edgar, R. C., Haas, B. J., Clemente, J. C., Quince, C. & Knight, R. UCHIME improves sensitivity and speed of chimera detection. *Bioinformatics* **27**, 2194–2200 (2011).
53. Edgar, R. C. Search and clustering orders of magnitude faster than BLAST. *Bioinformatics* **26**, 2460–2461 (2010).
54. Tsuda, A. et al. Influence of proton-pump inhibitors on the luminal microbiota in the gastrointestinal tract. *Clin. Transl Gastroenterol.* **6**, e89 (2015).
55. Segata, N. et al. Metagenomic biomarker discovery and explanation. *Genome Biol.* **12**, R60 (2011).
56. Ojiro, K. et al. MyD88-dependent pathway accelerates the liver damage of concanavalin A-induced hepatitis. *Biochem. Biophys. Res. Commun.* **399**, 744–749 (2010).
57. Hayashi, A. et al. A single strain of *Clostridium butyricum* induces intestinal IL-10-producing macrophages to suppress acute experimental colitis in mice. *Cell Host Microbe* **13**, 711–722 (2013).
58. Ondov, B. D. et al. Mash: fast genome and metagenome distance estimation using MinHash. *Genome Biol.* **17**, 132 (2016).
59. Brisse, S. et al. *wzi* Gene sequencing, a rapid method for determination of capsular type for *Klebsiella* strains. *J. Clin. Microbiol.* **51**, 4073–4078 (2013).
60. Pan, Y. J. et al. Capsular types of *Klebsiella pneumoniae* revisited by wzc sequencing. *PLoS ONE* **8**, e80670 (2013).

Acknowledgements

We thank S. Chiba, S. Shiba, R. Morikawa, T. Katayama, A. Ikura, Y. Mikami and T. Sujino (Division of Gastroenterology and Hepatology, Keio University) for technical assistance and critical reading of this manuscript. This study was supported by the Japan Society for the Promotion of Science (JSPS) KAKENHI Grant-in-Aid (C) 16K09374 and (A) 15H02534, the Advanced Research and Development Programs for Medical Innovation (AMED-CREST; 16gm1010003h0001), the TAKEDA Science Fund, Ezaki Glico Co. Ltd and Keio University Medical Fund. K.H. was funded through AMED LEAP under grant number JP17gm0010003. A. Yoshimura was supported by the JSPS KAKENHI Grant-in-Aid (S) JP17H06175, Challenging Research (P) JP18H05376 and AMED-CREST JP18gm0510019 and JP18gm1110009.

Author contributions

N.N. and T.K. designed the project. N.N., N.S., R.A., K.M., T.T., Takahiro S., Y.K., P.-S.C., N.T., Akihiro Y., M.K. and H.A. performed the experiments. W.S. and M.H. performed the bacterial sequence, microbiome analyses and contributed to data discussions. K.A., S.N. and K.H. provided essential materials and contributed to data discussions. N.N., N.K., M.S., Akihiko Y., Toshiro S. and T.K. interpreted the experimental data. N.N., N.K. and Toshiro S. wrote the manuscript. T.K. critically revised the manuscript and supervised the study.

Competing interests

The authors declare no competing interests.

Additional information

Supplementary information is available for this paper at https://doi.org/10.1038/s41564-018-0333-1.

Reprints and permissions information is available at www.nature.com/reprints.

Correspondence and requests for materials should be addressed to T.S. or T.K.

Publisher's note: Springer Nature remains neutral with regard to jurisdictional claims in published maps and institutional affiliations.

nature research

Corresponding author(s): Toshiro Sato

Reporting Summary

Nature Research wishes to improve the reproducibility of the work that we publish. This form provides structure for consistency and transparency in reporting. For further information on Nature Research policies, see Authors & Referees and the Editorial Policy Checklist.

Statistical parameters

When statistical analyses are reported, confirm that the following items are present in the relevant location (e.g. figure legend, table legend, main text, or Methods section).

n/a	Confirmed	
☐	☒	The exact sample size (*n*) for each experimental group/condition, given as a discrete number and unit of measurement
☐	☒	An indication of whether measurements were taken from distinct samples or whether the same sample was measured repeatedly
☐	☒	The statistical test(s) used AND whether they are one- or two-sided *Only common tests should be described solely by name; describe more complex techniques in the Methods section.*
☐	☒	A description of all covariates tested
☐	☒	A description of any assumptions or corrections, such as tests of normality and adjustment for multiple comparisons
☐	☒	A full description of the statistics including central tendency (e.g. means) or other basic estimates (e.g. regression coefficient) AND variation (e.g. standard deviation) or associated estimates of uncertainty (e.g. confidence intervals)
☐	☒	For null hypothesis testing, the test statistic (e.g. *F*, *t*, *r*) with confidence intervals, effect sizes, degrees of freedom and *P* value noted *Give P values as exact values whenever suitable.*
☒	☐	For Bayesian analysis, information on the choice of priors and Markov chain Monte Carlo settings
☒	☐	For hierarchical and complex designs, identification of the appropriate level for tests and full reporting of outcomes
☒	☐	Estimates of effect sizes (e.g. Cohen's *d*, Pearson's *r*), indicating how they were calculated
☐	☒	Clearly defined error bars *State explicitly what error bars represent (e.g. SD, SE, CI)*

Our web collection on statistics for biologists may be useful.

Software and code

Policy information about availability of computer code

Data collection	BD FACSDiva version 8.0.1 for flowcytometry
Data analysis	FlowJo v10 (Flow Jo LLC) for flowcytometry, QIIME software package v1.9.1, ea-utils software v1.1.2 for 16S rRNA analysis, Prism v7 (Graphpad) for the statistics, ImageJ 1.5.2a for quantitative analysis of the fibrotic area, and Tophat2 v2.1.1, Cufflinks v2.1.1, DAVID v6.8 for RNA-seq.

For manuscripts utilizing custom algorithms or software that are central to the research but not yet described in published literature, software must be made available to editors/reviewers upon request. We strongly encourage code deposition in a community repository (e.g. GitHub). See the Nature Research guidelines for submitting code & software for further information.

Data

Policy information about availability of data

All manuscripts must include a data availability statement. This statement should provide the following information, where applicable:

- Accession codes, unique identifiers, or web links for publicly available datasets
- A list of figures that have associated raw data
- A description of any restrictions on data availability

The data supporting the findings of this study are available from the corresponding author on request. 16S rRNA sequencing and whole genome sequencing data

have been deposited in the DNA Data Bank of Japan (DDBJ) database with accession numbers DRA007475 and DRA007476 for 16S rRNA sequencing, and PRJDB7545 for whole genome sequencing. RNA-sequencing data have been deposited in the European Genome-phenome Archive (EGA) database with accession number EGAS00001003332.

Field-specific reporting

Please select the best fit for your research. If you are not sure, read the appropriate sections before making your selection.

☒ Life sciences ☐ Behavioural & social sciences ☐ Ecological, evolutionary & environmental sciences

For a reference copy of the document with all sections, see nature.com/authors/policies/ReportingSummary-flat.pdf

Life sciences study design

All studies must disclose on these points even when the disclosure is negative.

Sample size	No statistical methods were used to predetermine sample sizes. Sample sizes were determined based on previous studies from our group and publications in the field.
Data exclusions	No data were excluded from the analysis
Replication	Experiments were replicated several times with reproducible results, as indicated in each figure legend.
Randomization	All animals used were age, sex and vendor matched. Animals were randomly allocated to each group.
Blinding	The data collection was not blinded. Blinding was not possible as the investigators were also conducting the experiments and had to be aware of controls and treated groups.

Reporting for specific materials, systems and methods

Materials & experimental systems

n/a	Involved in the study
☒	☐ Unique biological materials
☐	☒ Antibodies
☒	☐ Eukaryotic cell lines
☒	☐ Palaeontology
☐	☒ Animals and other organisms
☐	☒ Human research participants

Methods

n/a	Involved in the study
☒	☐ ChIP-seq
☐	☒ Flow cytometry
☒	☐ MRI-based neuroimaging

Antibodies

Antibodies used	anti-mouse anti-TCRb (no.109228, Biolegend, PerCP/Cy5.5 conjugate, clone H57-597), anti-CD3e (no.552774, BD bioscience, PE-cy7 conjugate, clone 145-2C11), anti-CD4 (no.563106, BD bioscience, BV510 conjugate, clone RM4-5), anti-CD11b (no.101245, Biolegend, BV510 conjugate, clone M1/70), anti-CD11c (no.558079, BDbioscience, PE-cy7 conjugate, clone HL3), anti-F4/80 (no.123131, Biolegend, BV421 conjugate, clone BM8), Fixable Viability Dye eFluor780 (no.65-0864-14, eBioscience), anti-IFN-g (no.554412, BD bioscience, PE conjugate, clone XMG1.2; no.11-7311-82, eBioscience, FITC conjugate, clone XMG1.2), anti-TNF-a (no.554419, BD bioscience, PE conjugate, clone MP6-XT22), anti-IL-1b (no.17-7114-80, eBioscience, APC conjugate, clone NJTEN3), anti-IL-17A (no.560221, eBioscience, Alexa Fluor488 conjugate, clone TC11-18H10), anti-IL-22 (no.17-7222-82, eBioscience, APC conjugate, clone IL22JOP), and anti-RORgt (no.562894, BD bioscience, BV421 conjugate, clone Q31-378).
Validation	All antibodies used in this study are from commercial sources and have been validated by the vendors. Validation data are available on the manufacturer's website (BD bioscience; https://www.bdbiosciences.com/eu/reagents/research/antibodies-buffers/immunology-reagents/c/744843, eBioscience; https://www.thermofisher.com/jp/en/home/life-science/cell-analysis/flow-cytometry/antibodies-for-flow-cytometry.html). Appropriate antibody dilutions were performed based on preliminary experiments.

Animals and other organisms

Policy information about studies involving animals; ARRIVE guidelines recommended for reporting animal research

Laboratory animals	Male GF mice (C57BL/6 background strain, 6-8-weeks old) were purchased from Sankyo Lab Service Corporation (Tokyo, Japan) and were kept in the GF Facility of Keio University School of Medicine. Male C57BL/6 mice (6-8-weeks old) were purchased from Japan CLEA (Tokyo, Japan) and maintained under specific pathogen-free (SPF) conditions in Central Laboratories for Experimental Animals (Kawasaki, Japan) and the Animal Care Facility of Keio University School of Medicine.
Wild animals	This study did not involve wild animals.
Field-collected samples	This study did not involve samples collected from the field.

Human research participants

Policy information about studies involving human research participants

Population characteristics	PSC/UC: 14 males/ 4 females, medial age 33 (20-69) UC: 13 males/ 3 females, median age 39 (21-63) AIH: 2 males/ 9 females, median age 51 (25-67) PBC: 3 males/ 7 females, median age 50 (40-68)
Recruitment	Human research participants were recruited in Keio University Hospital. Written, informed consent was obtained from all subjects. The study was approved by the ethics committee at Keio University School of Medicine (#20140211). The diagnosis of PSC was made according to clinical guidelines and typical findings on cholangiography (endoscopic retrograde cholangiography and/or magnetic resonance cholangiopancreatography) or liver biopsy. The diagnosis of UC was based on a combination of endoscopy, histopathology, and radiological and serological investigations. The diagnoses of AIH and PBC were made according to clinical guidelines and typical histological findings. There is no indication that self selection bias affected any of the results.

Flow Cytometry

Plots

Confirm that:

☒ The axis labels state the marker and fluorochrome used (e.g. CD4-FITC).

☒ The axis scales are clearly visible. Include numbers along axes only for bottom left plot of group (a 'group' is an analysis of identical markers).

☒ All plots are contour plots with outliers or pseudocolor plots.

☒ A numerical value for number of cells or percentage (with statistics) is provided.

Methodology

Sample preparation	sample preparation is listed in Methods
Instrument	BD FACSCanto™ II
Software	FACSDiva for collection and FlowJo (v10) for analysis
Cell population abundance	Populations were validated for purity by a post-sort analysis by FACS
Gating strategy	Every flow cytometry analysis was initiated as follows: FSC-A/SSC-A to gate the lymphocyte population Gating of the Fixble Viability Dye eFluor780 negative cells to select live cells followed by the gating as described in the figures.

☐ Tick this box to confirm that a figure exemplifying the gating strategy is provided in the Supplementary Information.